Aquaculture International (2026) 34:223
https://doi.org/10.1007/s10499-026-02622-y

RESEARCH

# Bacterial characterization of a disease event in larval rearing system of tropical rock lobster (*Panulirus ornatus*)

**Mengjia Jiang[1] · Andrew J. Trotter[1] · Ivona Mladineo[1,2] · Evan F. Goulden[3] · Gregory G. Smith[1]**

Received: 9 February 2026 / Accepted: 10 July 2026 / Published online: 23 July 2026


## Abstract

Disease outbreaks in commercial larval rearing systems of the tropical rock lobster (*Panulirus ornatus*) pose significant challenges to the culture of this species. This study investigates bacterial succession during outbreaks of white leg disease (WLD), the latter associated with infections by *Aquimarina* spp. in early-stage *P. ornatus* phyllosoma. Bacteriome profiling was conducted to assess changes in bacterial composition and identify potential sources of pathogenic taxa. Transmission electron microscopy was used to depict ultrastructural changes in the pereiopods of diseased specimens. Oxford Nanopore 16S rRNA gene sequencing was used to profile bacterial diversity and community structure across larval development (0–16 days post-hatch, dph), revealing temporal shifts coinciding with the onset of disease. A marked decline in alpha diversity between 8 and 16 dph was observed concomitant with an increase in diseased animals. During this period, the pathogenic genus *Aquimarina* became dominant, replacing early taxa such as *Vibrio*, *Ruegeria*, *Shimia*, and *Phaeobacter*, and concurring with massive coagulative necrosis and the subsequent formation of ellipsoid, electron-dense, proteinaceous bodies in pereiopod tissues. Beta diversity analysis further revealed significant shifts in community structure, implying that bacterial dysbiosis may be an early indicator of WLD development. The findings suggest that disease results from a combination of bacterial maternal or environmental transmission, environmental acquisition, and bacteria-bacteria interactions. The study highlights the importance of maintaining bacterial balance to support a healthy aquaculture system for larval lobsters, suggesting that early bacterial disruption can facilitate disease emergence.

Handling Editor: Daniel Merrifield

✉ Mengjia Jiang
Mengjia.jiang@utas.edu.au

[1] Institute for Marine and Antarctic Studies, University of Tasmania, PO Box 858, Sandy Bay, Hobart, TAS 7005, Australia

[2] Institute of Parasitology, Biology Centre Czech Academy of Sciences, Ceske Budejovice, Czech Republic

[3] Queensland Department of Primary Industries, Bribie Island Research Centre, Woorim, QLD 4507, Australia

**Highlights**

- The temporal bacterial shift in *Panulirus ornatus* coincided with white leg disease onset.
- *Aquimarina* dominated larvae at 16 dph, replacing early pioneer taxa.
- TEM showed necrosis and electron-dense bodies in diseased pereiopods.
- Infection pathways involved maternal and environmental sources.
- Bacterial interactions play an important role in pathogenesis.

**Keywords** Aquaculture · Tropical rock lobster (*Panulirus ornatus*) phyllosoma · White-leg disease (WLD) · Bacterial composition

## Introduction

The tropical rock lobster (*Panulirus ornatus*) is a highly valued seafood species with strong and increasing global demand (FAO 2024). Closed-cycle production of *P. ornatus* has recently been established, enabling the commencement of a commercial grow-out industry in Australia using hatchery-produced seedstock (Lewis et al. 2024). However, larval rearing of lobsters remains a major challenge due to their prolonged planktonic development, high nutritional demands, and complex environmental management requirements, all of which render larvae highly susceptible to pathogen-related risks (Driscoll et al. 2015; Francis et al. 2014; Goulden et al. 2013).

Bacterial diseases are a significant mortality factor in the larval rearing of palinurid lobsters. Experimental studies have demonstrated that *P. ornatus* phyllosoma are highly susceptible to *Vibrio owensii* (DY05), with mortality rates reaching 84–89% within 72 h (Goulden et al. 2012a). Similarly, *Vibrio jasicida* has been implicated in infections of the hepatopancreas in eastern rock lobster (*Sagmariasus verreauxi*, formerly *Jasus verreauxi*) phyllosoma, causing a rapid mortality (Bourne et al. 2007; Diggles et al. 2000). Other bacterial taxa, such as *Thiothrix* spp., have been reported to colonize gills and appendages, interfering with ecdysis and respiration and contributing to substantial mortality in hatchery systems (Payne et al. 2007). More recently, white-leg disease (WLD) has attracted increasing attention in *P. ornatus* hatcheries, exhibiting whitening of the pereiopods and uropods, reduced larval responsiveness, and rapid mortality (Ooi et al. 2020). Members of the genus *Aquimarina* have frequently been associated with WLD, recognized as etiological agents of tissue-degrading infections in a range of crustaceans (Midorikawa et al. 2020; Ooi et al. 2020).

These outbreaks underscore the vulnerability of larval stages and the acute threat posed by bacterial pathogens in intensive aquaculture systems. However, these earlier studies have focused on identifying individual pathogens, such as *Vibrio* spp. and *Aquimarina* spp., associated with disease using conventional microbiological techniques. Consequently, the broader bacterial community and dynamics associated with larval disease and mortality remain poorly understood for palinurid lobsters. Recent research on crustacean aquaculture species has highlighted that disease outcomes are often not caused by a single pathogen but rather arise from complex interactions among host-associated and environmental bacteria (Lu et al. 2022).

In early crustacean larval stages, bacteria contribute significantly to digestion, nutrient absorption, and immune development, while also acting as a protective barrier against opportunistic pathogens (Angthong et al. 2023; Dai et al. 2020). When this balance is disrupted by environmental stress, suboptimal nutrition, or physiological changes, bacterial

dysbiosis can occur, favoring the proliferation of pathogenic taxa (Egan and Gardiner 2016; Xiong et al. 2018b). Despite growing recognition of the contribution of bacteria to host health, a critical gap remains in understanding how bacterial communities shift during disease events in palinurid larviculture. In particular, the dynamics of bacterial succession during WLD outbreaks in *P. ornatus* larviculture, the roles of potentially pathogenic taxa, and the contributions of environmental reservoirs, such as tank water, biofilms, and feed, remain to be fully elucidated. Likewise, the type and development of lesions in affected tissues have not been previously described at the ultrastructural level. Understanding these aspects would improve knowledge of WLD pathogenesis and, in future, support the development of effective management strategies.

Therefore, this study aims to characterize the bacterial changes associated with mass disease events during the larval rearing of *P. ornatus*, focusing on identifying bacterial taxa linked to larval development, their temporal succession, and potential transmission pathways of key pathogens. It also depicts histopathological changes observed in diseased animals. By integrating Oxford Nanopore 16S rRNA sequencing of potential hatchery-related sources of infection throughout larval rearing, the research will elucidate the mechanisms driving larval disease outbreaks and candidate bacterial biomarkers for early disease detection, thereby facilitating the development of improved management strategies in tropical rock lobster aquaculture.

## Materials and methods

This study was conducted in a commercial-scale *P. ornatus* larval rearing system. As such, the study was not designed with predefined experimental treatments or uninfected control groups. Sampling was therefore undertaken following the accidental onset of WLD in larval tanks. Disease outbreaks in this system typically progress rapidly, resulting in mortality exceeding 75% of the larval population within a short timeframe, thereby precluding the establishment of contemporaneous healthy controls. Consequently, this study does not aim to infer causality or define dysbiosis relative to a healthy larval status, but rather to document bacteriome characteristics associated with a naturally occurring WLD outbreak in a commercial larval rearing system.

### Larval rearing

Rearing of *P. ornatus* broodstock and larvae was performed at the Institute for Marine and Antarctic Studies (IMAS), University of Tasmania, Taroona, Tasmania. Gravid females were placed in a hatchery tank supplied by seawater from a recirculating aquaculture system. No antibiotics or probiotics were applied in the broodstock or larval rearing systems prior to or during the outbreak period. Water quality parameters (mean ± SD) of the hatchery tank were temperature: 25.90 ± 0.03 °C; dissolved oxygen (DO): 94.05 ± 0.65%; pH: 7.97 ± 0.05; salinity: 35.1 ± 0.01 ppt (Fig. 1A). Female broodstock were held in the hatching tank until eggs hatched. Emergent larvae (0 days post-hatch, hereafter dph) were transferred to a specialized 0 dph larvae tank (Fig. 1B), before a second transfer to the 1–16 dph larvae tank (Fig. 1C). The rearing system water conditions (mean ± SD) of the larvae tank were temperature: 27.30 ± 0.10 °C; DO: 102.89 ± 0.31%; pH: 8.20 ± 0.01; salinity: 35.2 ± 0.01 ppt.

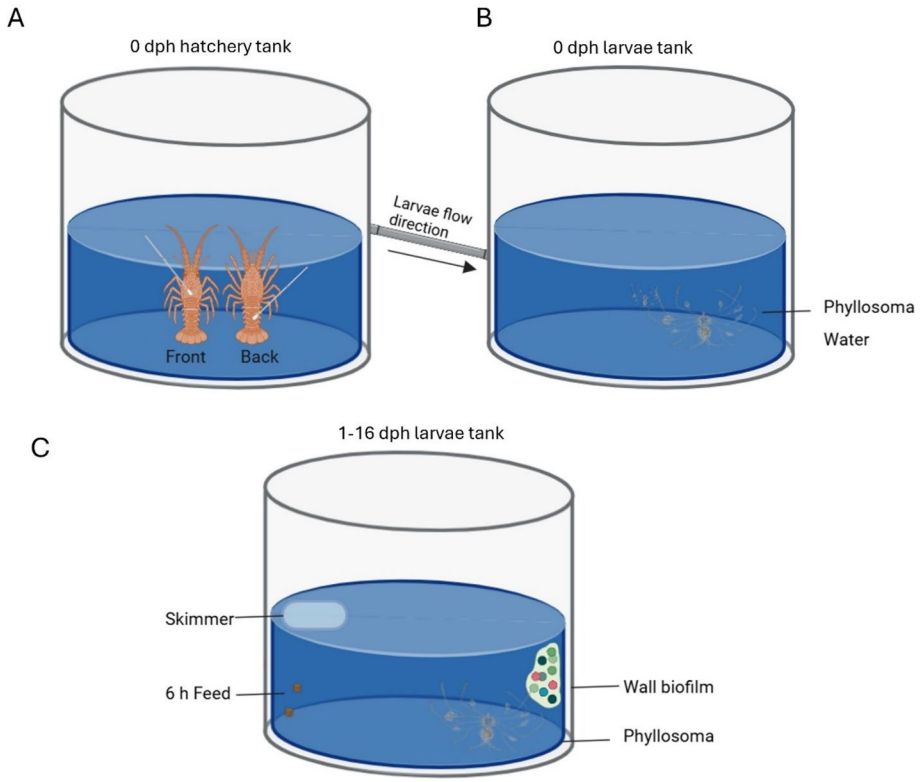


**Fig. 1** Schematic representation of sample collection sites during larval rearing of *Panulirus ornatus* at Taroona, Institute for Marine and Antarctic Studies, University of Tasmania, **A** 0 dph hatching tank, **B** 0 dph larvae tank, and (**C**) 1–16 dph larvae tank

## Broodstock and larval sample collection

Sampling was conducted at the onset of WLD, clinically diagnosed based on visible whitening of the articulated appendages, including the pereiopods, maxillipeds, antennae, and eyestalks, in accordance with the criteria described by Ooi et al. (2020). Samples from broodstock and phyllosoma were collected to characterize bacterial communities throughout the WLD outbreak and to examine gross and ultrastructural pathology during its peak. Female broodstock samples were collected from the pleopods and carapace of *P. ornatus* at 0 dph using sterile swabs from the 0 dph hatching tank (Fig. 1A) ($n = 3$). The swab was immediately placed into a 1.5 mL sterile plastic tube containing 500 µL of storage buffer (25 mM sodium citrate, 10 mM EDTA, 4 M ammonium sulfate, pH 5.2) and stored at 4 °C until further processing. Phyllosoma (0, 1, 8, and 16 dph) were collected from the 0 dph larvae tank and the 1–16 dph larvae tank, respectively ($n = 5$) (Fig. 1B, C) by sterile siphon and stored in 1.5 mL sterile plastic tubes (0–16 dph). The samples were first filtered using a 1.5 µm pore-size 47 mm Whatman GF/C glass microfiber filter (Cytiva, Whatman, UK) to remove residual water. Approximately 0.2 g of larvae was collected per sample, with five independent biological replicates per 0, 1, 8, 16 dph. Each sample was then transferred into a 1.5 mL tube containing 500 µL of storage buffer and stored at 4 °C overnight.

## Environmental sample collection

The environmental samples consisted of 6 h feed, which refers to feed offered to phyllosoma that remained uneaten within 6 h, thereby persisting in the water column prior to sampling; tank water; and swabs from the biofilm formed on the tank wall and skimmer. All environmental samples were collected in biological triplicate concurrently with phyllosoma samples, from 1 to 16 dph larvae tank (Fig. 1B and C). The 1–16 dph phyllosoma were fed a proprietary diet incorporating live *Artemia* (Sep-Art GSL *Artemia* cysts, INVE Aquaculture Inc., USA). The feed samples were collected after 6 h of immersion in tank water, i.e., these represented uneaten feed suspended in the rearing water column during this period. The feed was collected using a sterile Pasteur pipette and transferred to 1.5 mL sterile plastic tubes. Feed samples were then centrifuged at 12,000 × g to remove residual water, and the 0.02 g dry feed was stored in 500 µL of storage buffer. Tank water samples were collected into 1 L sterile glass bottles and filtered using a sterile 0.45 µm pore-size mesh membrane filter (Cytiva, Whatman) to capture bacterial cells (Hasegawa et al. 2003; Wang et al. 2007). The filter paper was cut into small pieces using flame-sterilized scissors and soaked in storage buffer. Biofilms on tank walls were sampled by swabbing a 10 $cm^2$ area and storing the swab in storage buffer. Similarly, the skimmer samples were collected by swabbing the surface area (10 $cm^2$) and storing the swab in a storage buffer. All samples in the buffer solution were stored at 4 °C for further processing.

The sample collection site summary figure (Fig. 1) was made using BioRender (BioRender.com).

## DNA extraction

Collected phyllosoma and environmental samples were processed using the same DNA extraction methods. Extraction was performed by adding 500 µL high-salt lysis buffer (1% SDS, 1.5 M NaCl, 0.1 M EDTA, 1% PVP-10), 5 µL of Proteinase K (Bioline Pty. Ltd., NSW, Australia) and 5 µL of tris(2-carboxyethyl)phosphine (T-CEP), 1 M. Samples were then heated at 65 °C for 1 h (vortexed every 20 min) and incubated on ice for 5 min. Ammonium acetate (7.5 M; Sigma-Aldrich Co., MO, USA) and potassium chloride were added to the samples at final concentrations of 2.5 M and 1 M, respectively, vortexed for 15 s, and centrifuged at 10,000 × g for 10 min at 22 °C. The supernatant was mixed by inversion with 750 µL of isopropanol with 1.5 µL iso-precipitant Co-Precipitant Pink (Bioline, London, UK) at room temperature before further centrifugation at 12,000 × g for 15 min at 22 °C. The visible pellet was rinsed with 500 µL of 70% ethanol twice and resuspended in 100 µL of buffered water (0.05% Triton X-100, 10 mM TRIS pH 7). RNA was removed by digesting the sample with 2 µL of RNase A (10 mg/ml, Thermo Fisher, USA) at 37 °C for 30 min. Samples were treated with 200 µL of ammonium acetate (2.5 M), 200 µL of 1 M Potassium chloride, and 400 µL high-salt lysis buffer, vortexed for 30 s, and centrifuged at 10,000 × g for 10 min (22 °C). The supernatant was mixed with an equal volume of isopropanol with co-precipitant pink and centrifuged at 12,000 × g for 15 min. The pellet was rinsed with 70% ethanol twice before resuspension in 50 µL of molecular-grade water (Qiagen, Germany). All samples were quantified by Qubit 4 (Thermo Scientific, USA) using the Qubit 1 × dsDNA BR Assay Kit (Thermo Scientific, USA) following the manufacturer's instructions.

## Quantitative PCR, library preparation, and 16S rRNA sequencing on the MinION platform

### Pre-amplification

All the samples were pre-amplified by qPCR targeting the 16S rRNA locus (Matsuo 2023; Ooi et al. 2023). The primary SYBR Green qPCR mixture consisted of 5 µL of 2 × MyTaq Hot Start mix (Bioline, Meridian Bioscience, USA), 100 mM each of 27 F (5′-AGAGTT TGATCMTGGCTCAG-3′) and 1492R (5′-GGTTACCTTGTTACGACTT-3′) 16S rRNA primers (melting curve temperature $T_m$ between 86 and 88 °C) (Ooi et al. 2023), 2 µL of 1:10 diluted DNA, and 2 µL of molecular water. The qPCR was conducted using a Thermal Cycler (Bio-Rad Laboratories Inc., USA) with the following thermal cycling program: initial denaturation for 3 min at 95 °C; 35 cycles of denaturation for 10 s at 95 °C, annealing for 30 s at 55 °C, extension for 30 s at 72 °C; and a final extension for 3 min at 72 °C. Amplified DNA was purified using AMPure XP beads (Beckman Coulter, Indianapolis, IN, USA) with a 1:1.8 wash ratio, following the manufacturer's instructions (AMPure XP DNA Cleanup Workflow). The final cleaned DNA was additionally quantified by Qubit 4.

### Library preparation

The library preparation mixture consisted of 10 ng of input DNA, adjusted to a total of 15 µL with molecular water, 25 µL Long Amp Hot Start Taq 2X Master Mix (New England Biolabs, Ipswich, MA, USA), and 10 µL of unique 16S barcode (16S Barcoding kit, SQK 16S 114.24, Oxford Nanopore Company, UK). The qPCR was conducted using a Thermal Cycler (Bio-Rad Laboratories Inc., USA) with the following thermal cycling program: initial denaturation for 1 min at 95 °C; 25 cycles of denaturation for 25 s at 95 °C, annealing for 25 s at 55 °C, extension for 25 s at 65 °C; and a final extension for 5 min at 65 °C. EDTA (1 µL) was added to each sample to stop the reaction. Amplified DNA was purified using AMPure XP beads (Beckman Coulter, Indianapolis, IN, USA) with a 1:1.8 wash ratio, following the manufacturer's instructions (AMPure XP DNA Cleanup Workflow). The final cleaned DNA was additionally quantified by Qubit 4.

### Priming and sequencing

After library preparation, a total of 50 ng of DNA was pooled together from the last step, then incubated with 1 µL of a mixture of Rapid Adapter (RA) and Adapter Buffer (AB) at room temperature for 5 min. The prepared DNA pool library was mixed with 34 µL of Sequencing Buffer (SQB), 25.5 µL of Loading Beads (LB), and 4.5 µL of molecular-grade water, loaded onto the SpotON R10.4.1 flow cell (Oxford Nanopore Technologies, UK) for 48 h, and sequenced on the MinION™ Mk 1C. The generated sequencing data were monitored in real-time using the MinKNOW software (version 4.0.20). A total of three flow cells has been used, each containing 20, 20, or 22 samples. As a control, the DNA of a microbial community (Zymo Biomics Microbial Community Standard) was included in the sequencing runs (Supplement Table 3, Representative result).

### Gross clinical changes

The 16 dph specimens with visible changes in the pereiopods were collected from the larval tank using a disposable Pasteur pipette and immediately transferred for microscopy. Specimens were examined as native wet mounts in a small Petri dish containing filtered tank seawater to preserve the natural transparency of unaffected body parts in contrast to altered tissues, using a Leica M165C stereomicroscope equipped with a Leica DMC4500 camera at 40 × magnification.

### Transmission electron microscopy of infected phyllosoma

Three specimens showing no clinical signs of WLD and three specimens (16 dph) with visible changes in the pereiopods were collected from the larval tank using a Pasteur pipette, and immediately fixed in 3% glutaraldehyde in 0.22 µm filtered seawater for 4 h at 4 °C. The central part of the lesion was deliberately targeted for TEM to ensure capturing the complete extent of tissue damage. Sections have been selected as a subset of the most informative samples (specimens with very conspicuous lesions vs specimens with no lesions observed by light microscopy), and the most representative have been presented. The samples were washed three times in 0.22 µm-filtered seawater, then fixed in 1% aqueous osmium tetroxide, and washed twice more in the filtered seawater. Samples were dehydrated in ascending ethanol concentrations (70% × 1, 95% × 2, 100% × 3) and propylene oxide (× 2), then infiltrated in resin (EMBed 812, EMS, USA); first with 50% propylene oxide, then in pure resin overnight. The next day, samples were embedded in fresh resin and polymerized at 60 °C for 48 h. Semi-thin sections (500 nm) for orientational purposes were cut using an ultramicrotome (Leica, Germany), stained with toluidine blue, heated on a hotplate (60 °C), and checked under the light microscope Zeiss Axio Lab.A1 (Zeiss, Germany). Ultrathin sections (100 nm) were laid on formvar-coated copper grids, secondarily stained with uranyl acetate and lead citrate, and examined by a Hitachi HT7700 microscope operating at 80 kV equipped with a CCD camera.

### Bioinformatics and data analysis

Dorado software ver. 0.7.1 (Oxford Nanopore Technologies, https://github.com/nanoporetech/dorado) with the "evolution" basecalling model was used for basecalling the sequencing data (POD5 files) to generate FASTQ files with a mean quality score > 10, reads demultiplexing, and trimming of adapters and primers. Subsequently, reads were filtered using NanoFilt ver. 2.8.0, retaining reads between 1200 and 1700 bp, and the taxonomic profiling was performed using EMU (Curry et al. 2024, 2022) with the NCBI 16S database.

After taxonomic assignment, a table of assigned reads for each sample was uploaded to Microbiome Analyst (Lu et al. 2023) to calculate relative abundances. Data were filtered to remove low-abundance and low-prevalence features, with a minimum count threshold of 4 and a minimum sample prevalence of 20% (Ooi et al. 2023). Samples were rarefied to the minimum library size to standardize sequencing depth, and total sum scaling was applied to normalize read counts prior to diversity and compositional analyses (Ooi et al. 2023). The relative abundance of bacteria was then computed at the family and genus levels.

Alpha diversity of bacterial communities was assessed using Observed and Shannon indices to evaluate species richness and evenness across experimental groups. All

analyses were conducted in R (version 4.4.3) using the vegan package, and visualization of alpha diversity was performed using bar plots with ggplot2 (Wickham et al. 2025). Differences in samples across time points were assessed using the Kruskal–Wallis test. When significant, post-hoc pairwise comparisons were conducted using the Wilcoxon rank-sum test with a Benjamini–Hochberg (BH) correction for multiple testing, implemented in the rstatix package (Kassambara 2019). For each alpha diversity metric, summary statistics (mean ± standard deviation) were calculated for each group. Statistically significant differences between groups were highlighted on the plots using *p*-value–based significance codes (ns: not significant, *: $p < 0.01$, **: $p < 0.001$).

For beta diversity, dispersion among groups was assessed using PERMDISP (Anderson 2006), which revealed no significant differences ($p = 0.11$), supporting the assumption of homogeneity of variance and justifying the use of PERMANOVA (Anderson 2001) to test for compositional differences. PERMANOVA was subsequently performed to evaluate differences in bacterial community composition between groups. Pairwise comparisons were conducted using pairwise.adonis2 (Martinez Arbizu 2020; Oksanen et al. 2025) in *R*, with *p*-values adjusted for multiple testing using the Benjamini–Hochberg method (Benjamini and Hochberg 1995). The pairwise distance matrix of the bacterial community dataset was visualized using Principal Coordinates Analysis (PCoA) based on Bray–Curtis distances (Shi et al. 2020), with samples colored according to experimental group. For bacterial correlation analysis, the 10 most abundant taxa were selected, and counts were converted to relative abundances. Spearman correlations were calculated between taxa; correlations below 0.1 or self-correlations were removed, and an undirected network was constructed with nodes sized by degree and node pies representing relative abundance across days post-hatch groups. Node coordinates were computed using the Fruchterman-Reingold layout with absolute edge weights, produced in R 4.4.3.

Shared and unique bacterial genera among the samples were identified, and Venn diagrams were produced using InteraciVenn (Heberle et al. 2015). The correlation and linear discriminant analysis (LDA) plot were generated using the Microbiome Analyst software. The linear discriminant analysis effect size (LEfSe) plot was generated using an LDA score threshold of 6.0 at the genus level and a *p*-value cutoff of 0.05 with FDR adjustment (Lu et al. 2023).

## Results

### Gross and ultrastructural changes in diseased phyllosoma

The most striking gross change exhibited as a white, opaque discoloration localized to the appendages, particularly affecting the second and third pereiopods (Pe), which showed diffuse whitening along their entire length (Fig. 2). Lesions were initially observed as small focal opacities at the articulated joints, especially near the basis (Bs) and ischio-merus (Is-Me) segments, suggesting that infection may have originated through the arthrodial membranes. These are thin, flexible regions that are vulnerable to microbial entry. As the condition progressed, whitening extended distally into the exopod (Expd) and other limb regions. The white lesions presented as sharply demarcated zones of opacity, disrupting the typically transparent appearance of healthy limbs.

In the healthy phyllosoma, slow- and fast-twitching myofibrils are distinct in the pereiopod myocytes, the former enriched in actin fibers (Fig. 3A). Mitochondria are conspicuous,

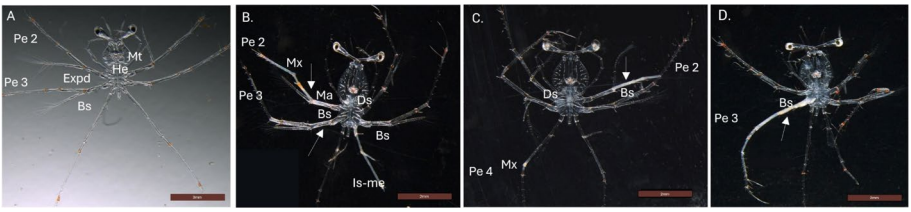


**Fig. 2** Gross pathological changes (arrows) showing typical progression of white leg disease (WLD) at 16 day post hatch (stage III–IV) of *Panulirus ornatus* larvae: **A** Healthy phyllosoma; **B** White lesion at basis (Bs), ischio-merus (Is-me), and exopod (Expd) of the pereiopods (Pe) 2 and 3; **C** White lesion at basis (Bs) at pereiopod 2 and body; and (**D**) White lesion at basis (Bs) and throughout the pereiopods 3 and whole exopod. Scale bars: **A** 3 mm; **B**–**D** 2 mm

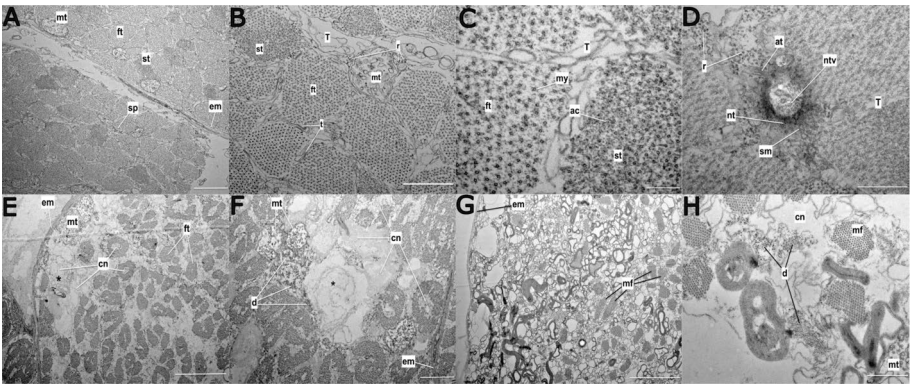


**Fig. 3** Representative pictures of the transmission electron microscopy of phyllosoma showing no gross changes ($n = 3$, **A**–**D**) and phyllosoma showing changes ($n = 3$, **E**–**H**) during a white leg disease outbreak. **A** Slow-twitching myofibrils are interspersed among fast-twitching myofibrils, both tightly packed within the endomysium; **B** Higher magnification of myocyte sarcoplasmic reticulum connected to T-tubules in a triad. Note scattered ribosomes surrounding a mitochondrion with tubular cristae; **C** Actin and myosin structures in slow- and fast-twitching myofibrils; **D** Neuromuscular junction consisting of an axon terminal, synaptic cleft, and a myocyte postsynaptic membrane; **E** Coagulative necrosis presented among and centrally in the myofibrils of the pereiopods. Note the changes ranging from the rarefaction of the sarcoplasm to formation of electron-dense ellipsoid structures (*); **F** Higher magnification of necrotic change showing degraded myofibrils adjacent to two mitochondria; **G** In progressed changes, the myofibrils are substituted by ellipsoid, proteinaceous structures of different electron density, and the endomysium is intact; **H** Electron-light proteinaceous structures filled with similar material adjacent to degraded myofibrils. ac, actin; at, axon terminal; cn, coagulative necrosis; d, degraded myofibrils; em, endomysium; ft, fast-twitching myofibrils; mt, mitochondrion; my, myosin; nt, neurotransmitters; ntv, neurotransmitter vacuole; r, ribosomes; sm, postsynaptic membrane; sp, sarcoplasm; st, slow-twitching myofibrils; T, T-tubule; t, triad. Scale bars: **C**, **D** 500 nm; **B**, **H** 1 mm; **A**, **F** 2 mm; **E**, **G** 5 mm

mostly with elongated tubular cristae (Fig. 3A). Myocyte triads and T-tubules are well developed (Fig. 3B and C), and the neuromuscular junctions are visible (Fig. 3D). In affected phyllosoma, the sarcoplasm of myocytes undergoes extensive coagulative necrosis (Fig. 3E), encompassing rarefaction of the sarcoplasm (Fig. 3F) and the formation of irregular, ellipsoid, proteinaceous aggregates that increase in size and change from electron-light to electron-dense structures (Fig. 3G). The necrotic changes in the myofibrils start centrally, progressing to a disorganized fiber structure without clear myosin-actin

boundaries, ultimately resulting in degraded fibers (Fig. 3H). The ellipsoid aggregating structures initially encompass some electron-light material, but as the process progresses, they become vacuolated (Fig. 3G and H). T-tubules and myocyte triads are not observed, although the endomysium is clearly present. In selected sections, no bacterial cells were observed.

## Alpha and Beta-diversity of larval bacterial communities

The alpha diversity of bacterial communities was assessed using the Kruskal–Wallis test, and changed throughout larval development, with Observed and Shannon indices showing a general decrease from 0 to 16 dph (Fig. 4). While both indices were statistically similar between 0 and 1 dph, they sharply declined by 16 dph. The 16 dph differed from all other time points in alpha diversity, but 8 dph differed from 0 and 1 dph in Shannon index.

Beta-diversity visualized in PCoA showed that PCoA1 and PCoA2 accounted for 38.8% and 17.5% of the variation, respectively, indicating that larval bacterial communities differed significantly from one another. There were significant differences ($p = 0.004$) at the genus level among bacterial communities across 0–16 dph larvae (Fig. 5). Pairwise comparisons indicated the strongest differences in community dispersion between 1 and 16 dph ($p = 0.007$), and between 8 and 16 dph ($p = 0.011$).

The taxonomic composition of bacterial communities associated with *P. ornatus* larvae changed measurably over time. At the family level, larvae at 0 dph were dominated by Haliscomenobacteraceae (17.0%) and Vibrionaceae (22.5%). By 1 dph, Roseobacteraceae (26.0%) and Flavobacteriaceae (11.6%) became most abundant. At 8 dph, the community was strongly dominated by Vibrionaceae (71.6%), before shifting again to Flavobacteriaceae (82.6%) at 16 dph (Fig. 6A, Supplement Table 1).

At the genus level, *Portibacter* (11.5%) and *Phaeodactylibacter* (5.5%) characterized larvae at 0 dph. By 1 dph, *Ruegeria* (11.9%), *Alteromonas* (9.9%), and *Marinibactrum* (8.8%) were more abundant. *Vibrio* dominated at 8 dph (71.6%), while *Aquimarina* became overwhelmingly dominant at 16 dph (82.5%) (Fig. 6B, Supplement Table 1).

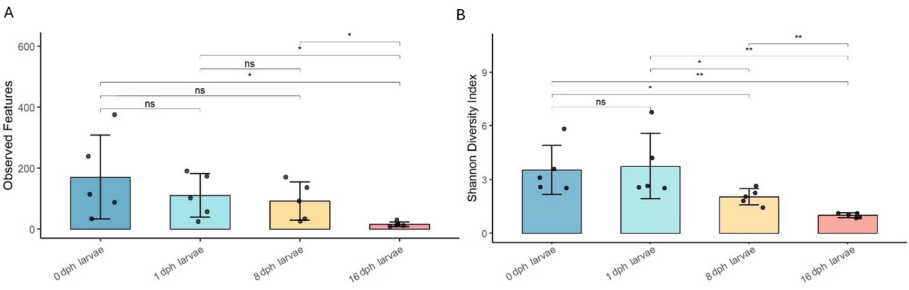


**Fig. 4** Barplot showing comparisons of alpha diversity indices of bacterial communities associated with *Panulirus ornatus* larvae (0–16 dph), based on five biological replicates per stage ($n = 5$). **A** Observed richness, and (**B**) Shannon diversity index as an estimate for species abundance. Bar heights represent the mean values, with error bars indicating standard deviation (SD). Asterisks (*) denote statistically significant differences between groups, *$p < 0.01$, **$p < 0.001$; ns, no significant differences

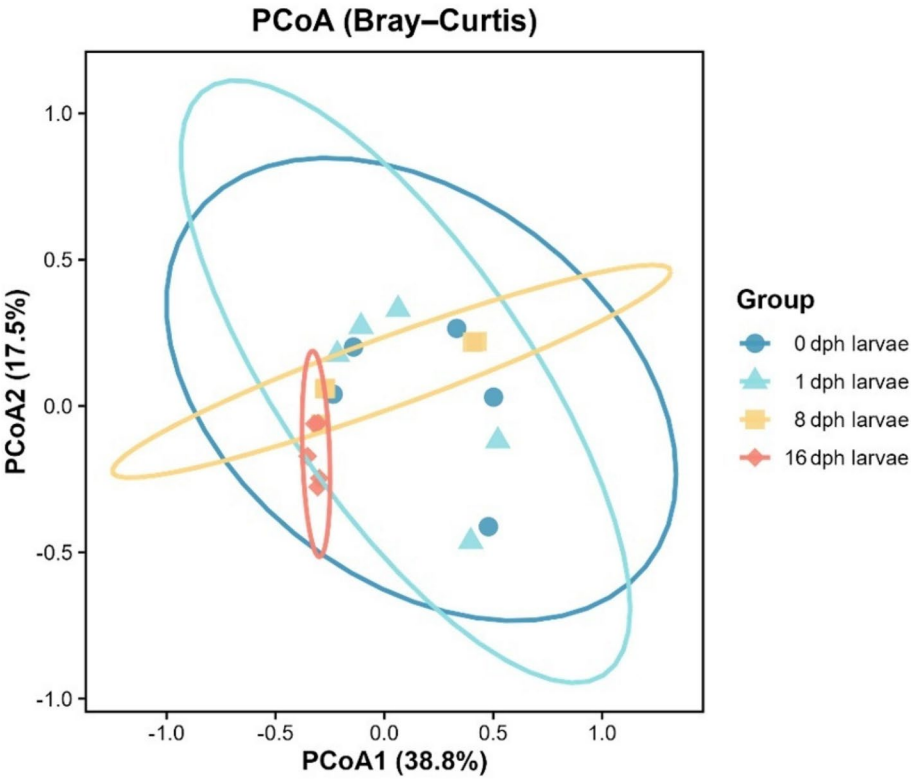


**Fig. 5** Principal coordinate analysis (PCoA) showing similarity in *Panulirus ornatus* larval bacterial communities (0–16 dph, $n = 5$) at the genus level

## Correlation network patterns of larval bacterial communities

The network analysis revealed a complex web of interactions among bacterial communities across all larval stages (0–16 dph). The families Vibrionaceae and Flavobacteriaceae emerged as key taxa (−0.68) (Fig. 7). Vibrionaceae showed a direct and strong negative correlation with several bacterial families, including Rhodobacteraceae (−0.31), Roseobacteraceae (−0.31), and Alteromonadaceae (−0.18), but positive correlation with Pseudoalteromonadaceae (+0.48) and Colwelliaceae (+0.39) (Fig. 7). Flavobacteriaceae also displayed direct negative associations with Alteromonadaceae (−0.35), Oceanospirillaceae (−0.59).

## Unique and shared bacterial taxa across broodstock, larvae, and the rearing environment

Larvae shared taxa with both broodstock and the rearing environment across 0–16 dph, highlighting potential microbial sources (Fig. 8). At 0 dph, larvae shared more taxa with broodstock ($n = 282$) and rearing water ($n = 129$), including *Aquimarina* sp., *Ruegeria* sp. AD91A and *Shimia* sp. (Supplement Table 2). Larvae at 0 dph had the greatest number of

**Fig. 6** Relative abundance of major bacterial communities at (**A**) family level, and (**B**) genus level associated with *Panulirus ornatus* larvae (0–16 dph, $n=5$). Data are represented by more than 1% of the reads in at least one sample, with other reads grouped into "others classification"

unique taxa ($n=192$) compared with 1–16 dph larvae (Fig. 8). At 1 dph, larvae exhibited the highest number of taxa and acquired for the first time, taxa shared with tank biofilm ($n=131$), skimmer ($n=155$), and feed ($n=104$) (Fig. 8). Following 1 dph, the total number of bacterial taxa on larvae generally decreased from 704 at 1 dph to 95 at 16 dph (Fig. 8). Similarly, the number of bacterial taxa found on larval samples and shared with broodstock and the environment also decreased with time. At 1 dph, larvae, water, and feed shared 69 taxa, including *Aquimarina* sp., *Vibrio* sp., and *Alteromonas* sp. (Supplement Table 2). Bacterial abundance decreased after 1 dph; at 8 dph, larvae mostly shared bacteria with water ($n=91$) and the surface skimmer ($n=86$), with *Vibrio* sp., *Pseudoalteromonas* sp., and *Phaeobacter* sp. being the most abundant (Supplement Table 2). Larvae at 16 dph had the lowest number of unique bacterial species ($n=4$), with a total of six species shared in all groups, including *Aquimarina* sp., *Vibrio* sp., *Alteromonas* sp., *Laceyella* sp., *Neptuniibacter* sp., and *Tateyamaria* sp. (Supplement Table 2).

### Bacteria composition across broodstock, phyllosoma and surrounding environments

The beta diversity metrics illustrate different clustering patterns and significant differences between broodstock, larvae, and the environment. At 0 dph, all bacterial communities clustered separately ($p=0.07$) (Fig. 9). At 1 dph, the larval bacterial communities were similar to feed samples ($p=0.372$), however, significant differences were detected among samples from the other rearing environments ($p=0.02$; Fig. 9B). At dph 8, larval bacterial communities differed significantly from the environment ($p=0.04$; Fig. 9C). By 16 dph, bacterial communities were widely distributed along both axes, with larvae and environmental samples positioned distinctly from other sources ($p=0.02$; Fig. 9D).

LEfSe analysis identified key bacterial taxa differentiating sample groups, with several taxa exceeding the LDA score threshold of 6.0 (Fig. 10). The genera included *Vibrio*, *Aquimarina*, *Ruegeria*, *Neptuniibacter*, *Aquihabitans*, *Shimia*, and *Marinibactrum*. *Vibrio* was most abundant in 8 dph larvae and was further significantly elevated above levels for the rearing environment at the same time point (Fig. 10). Additionally, *Vibrio* was more abundant in 0 dph larvae, and 8 dph and 16 dph feed. Notably, *Aquimarina* was significantly more enriched in larval samples compared to the rearing environment, particularly at 16 dph (Fig. 10). *Ruegeria* was predominantly enriched in early stages of larval rearing (0–1 dph) and was significantly elevated in rearing water and biofilms (Fig. 10). In contrast, *Shimia* and *Marinibactrum* were primarily found in 1 dph feed, biofilm, and larvae-associated environments. Genera *Spongiibacter*, *Thalassococcus*, *Phaeobacter*, and *Maritalea* were present in lower abundance across all samples but showed higher enrichment in 1 dph larvae and environment-associated bacteria.

## Discussion

Understanding the bacterial dynamics associated with larval disease in *P. ornatus* cultured within a research hatchery operating a commercial-scale system is crucial for improving system design, husbandry practices, and larval survival. This longitudinal study examined

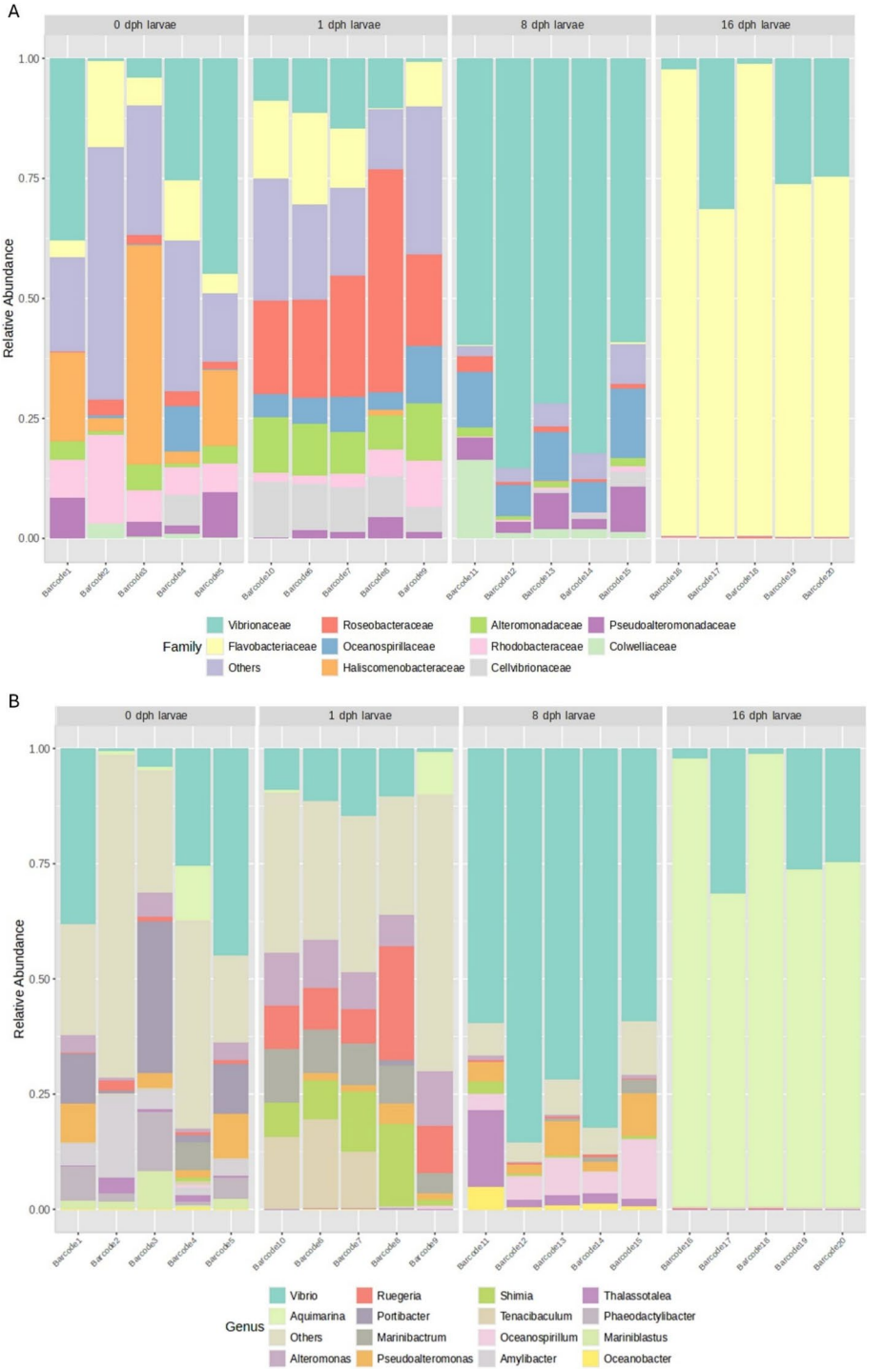
A
0 dph larvae
1 dph larvae
8 dph larvae
16 dph larvae
Relative Abundance
1.00
0.75
0.50
0.25
0.00
Barcode1
Barcode2
Barcode3
Barcode4
Barcode5
Barcode10
Barcode6
Barcode7
Barcode8
Barcode9
Barcode11
Barcode12
Barcode13
Barcode14
Barcode15
Barcode16
Barcode17
Barcode18
Barcode19
Barcode20
Family
Vibrionaceae
Flavobacteriaceae
Others
Roseobacteraceae
Oceanospirillaceae
Haliscomenobacteraceae
Alteromonadaceae
Rhodobacteraceae
Cellvibrionaceae
Pseudoalteromonadaceae
Colwelliaceae
B
0 dph larvae
1 dph larvae
8 dph larvae
16 dph larvae
Relative Abundance
1.00
0.75
0.50
0.25
0.00
Barcode1
Barcode2
Barcode3
Barcode4
Barcode5
Barcode10
Barcode6
Barcode7
Barcode8
Barcode9
Barcode11
Barcode12
Barcode13
Barcode14
Barcode15
Barcode16
Barcode17
Barcode18
Barcode19
Barcode20
Genus
Vibrio
Aquimarina
Others
Alteromonas
Ruegeria
Portibacter
Marinibactrum
Pseudoalteromonas
Shimia
Tenacibaculum
Oceanospirillum
Amylibacter
Thalassotalea
Phaeodactylibacter
Mariniblastus
Oceanobacter

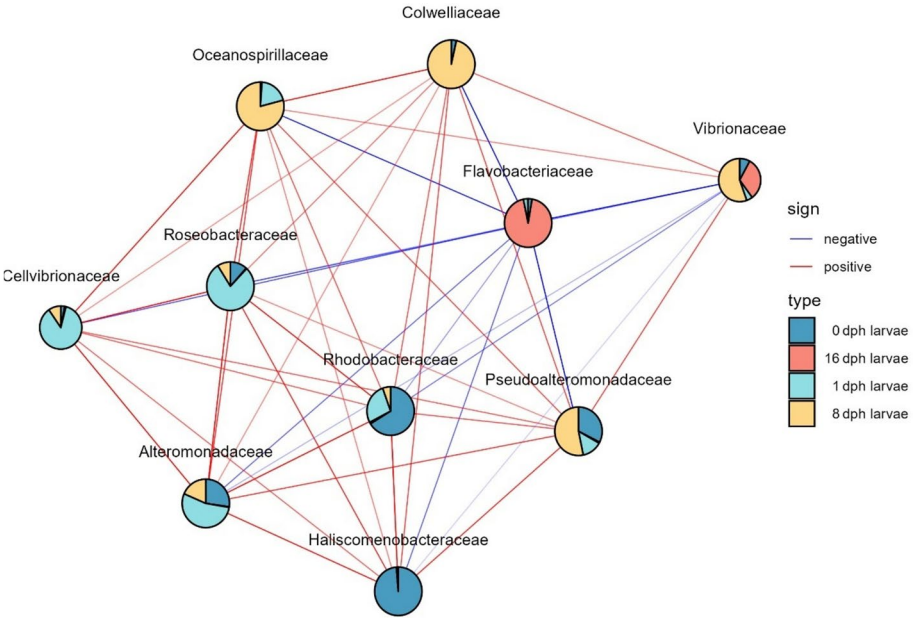


**Fig. 7** Correlation network analysis of *Panulirus ornatus* larvae bacterial communities at the family level across 0–16 dph, $n=5$. Edges represent significant pairwise correlations based on Spearman's rank analysis. Positive correlations are shown in orange (co-occurrence), and negative correlations in blue (mutual exclusion)

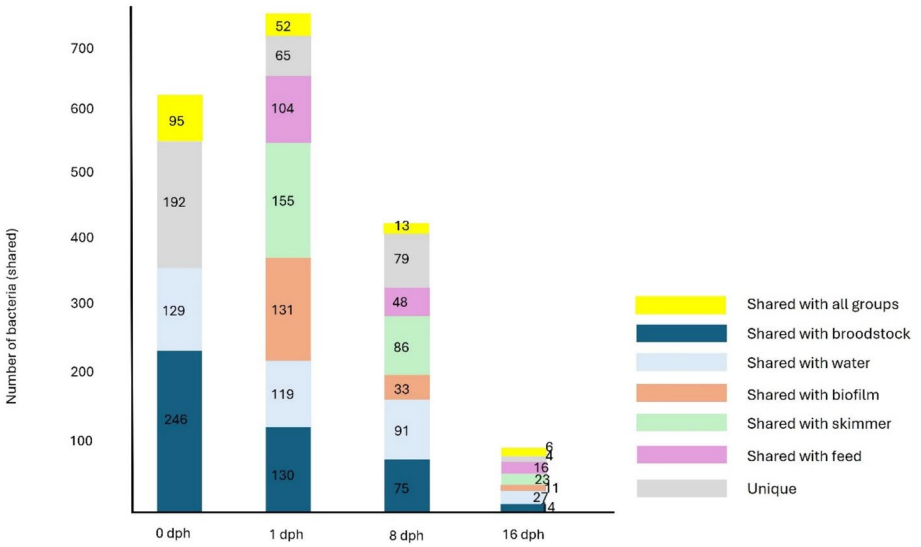


**Fig. 8** Number of shared and unique operational taxonomic units among *Panulirus ornatus* larvae and surrounding environments across 0–16 dph, calculated at the species level. Sample sizes were as follows: at 0 dph: larvae ($n=5$ per stage); broodstock ($n=3$, for 0 dph only); water ($n=3$); biofilm ($n=3$); skimmer ($n=3$); and feed ($n=3$)

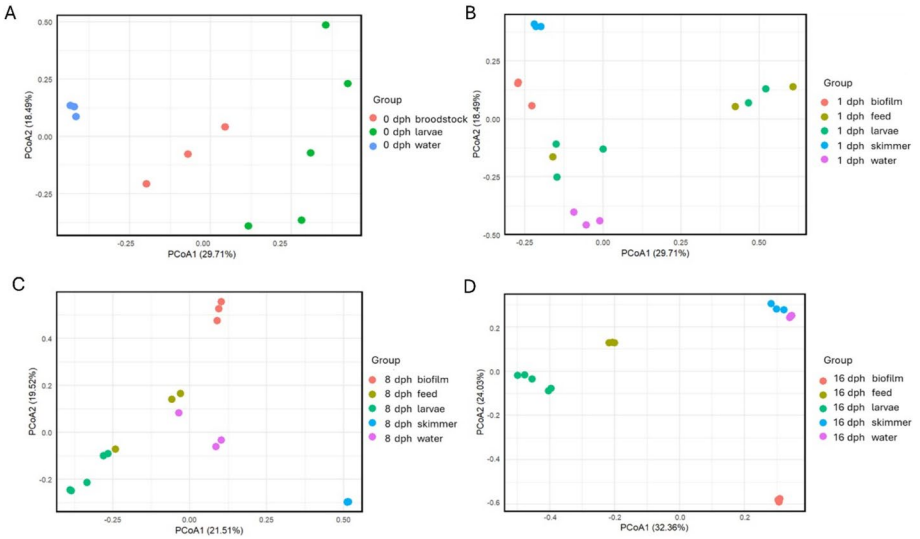


**Fig. 9** Beta diversity of *Panulirus ornatus* larvae, broodstock, and rearing environment (water, feed, surface skimmer, biofilm) across 0–16 dph. **A** 0 dph (larvae: $n=5$; broodstock: $n=3$; water: $n=3$); **B** 1 dph (larvae: $n=5$; biofilm, water, feed, and skimmer: $n=3$ each); **C** 8 dph (larvae: $n=5$; biofilm, water, feed, and skimmer: $n=3$ each); and (**D**) 16 dph (larvae: $n=5$; biofilm, water, feed, and skimmer: $n=3$ each)

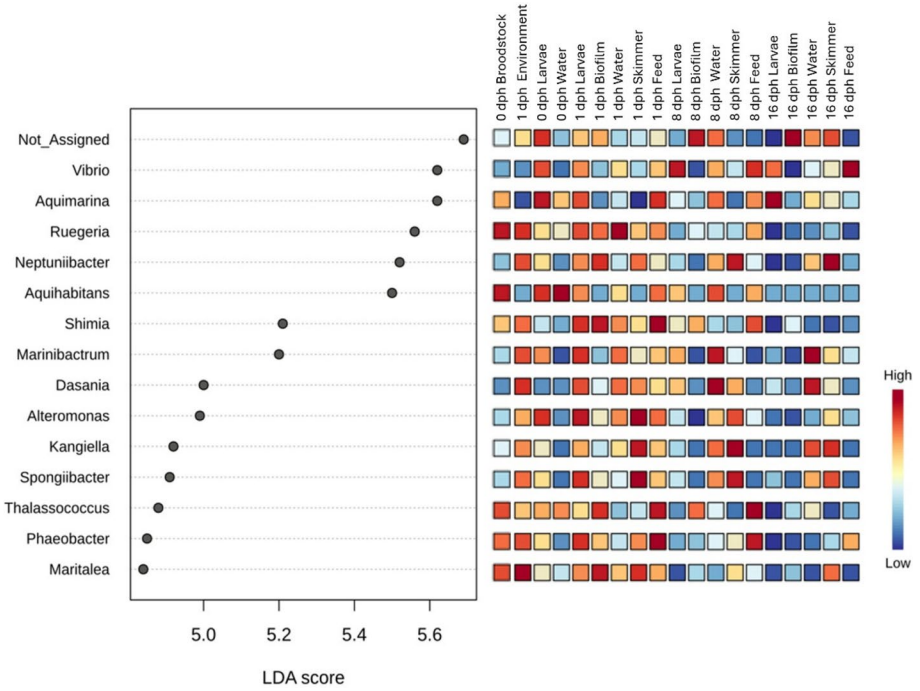


**Fig. 10** Linear discriminant analysis effect size (LEfSe) performed on the bacterial community relative abundance of *Panulirus ornatus* larvae, broodstock, and rearing environment between 1 and 16 dph

the composition, succession, and interactions of bacterial communities throughout early larval development and at the onset of WLD, as well as the gross and ultrastructural pathology associated with the disease. This study shows that dysbiosis and increased relative abundance of potentially pathogenic taxa are associated with disease onset in cultured lobster larvae.

The composition and diversity of microbial communities are critical for maintaining physiological balance and disease resistance in aquatic animals. A stable bacterial community has been proposed to support host health and disease resistance (Cassol et al. 2025; Xiong et al. 2017). In contrast, a reduction in bacterial diversity often reflects a dysbiosis state and may indicate increased disease susceptibility, potentially due to the loss of beneficial or antagonistic bacterial taxa (Xiong et al. 2018b). We observed a significant decline in bacterial alpha diversity between 0 and 1 dph and 8 and 16 dph, coinciding with the onset and increased incidence of WLD in *P. ornatus* larvae. While this may be indicative of a disease-associated microbial shift, a controlled experiment should elucidate whether a naturally occurring maternal-to-environmental bacteria succession could have contributed to the observed shift in larvae. The early loss of diversity at 1 dph may reflect rapid environmental filtering following hatching and transfer into the rearing system, rather than an early disease-specific signal. This temporal shift and the peak in WLD within the system suggest an association between alterations in community structure and disease. Similar associations between reduced bacterial diversity and disease have been reported in other aquaculture species infected with bacterial diseases, such as furunculosis in the largemouth bronze gudgeon (*Coreius guichenoti*) (Li et al. 2016) and acute hepatopancreatic necrosis disease (AHPND) in the white leg shrimp (*Litopenaeus vannamei*) (Cassol et al. 2025; Xiong et al. 2018a, 2017).

The species composition (beta diversity) changed with larval development and the onset of WLD in *P. ornatus*. At 0–1 dph, larval bacterial communities were dominated by Roseobacteraceae, Alteromonadaceae, and Haliscomenobacteraceae, which have been previously reported to be associated with host-associated functions, although their function in this system remains uncertain. Roseobacteraceae and Alteromonadaceae are commonly found in the hepatopancreas and gut of lobster, some members of which are known to contribute to organic compound degradation and bioactive substance production, potentially supporting digestion in lobsters (Feinman et al. 2017; Ooi et al. 2023). Members of the family Haliscomenobacteraceae are commonly associated with biofloc technology systems, contributing to biofloc formation, nutrient cycling, and water purification (Lu et al. 2022; Rajeev et al. 2024). Members of the genera within the Alphaproteobacteria (*Shimia* spp., *Phaeobacter* spp., *Ruegeria* spp.) were most abundant during early larval stages. Alphaproteobacteria are strongly represented in bacterial assemblages of wild *P. ornatus* phyllosoma, and some species display antagonistic activity against pathogenic vibrios in cultured phyllosoma (Goulden et al. 2013; Payne et al. 2008). *Shimia* spp. are known to contribute to bacterial stability, biofilm formation, osmoregulation and protein metabolism, thereby potentially supporting early larval nutrition and survival (Hyun et al. 2013; Zhang and Sun 2022). *Phaeobacter* spp. are commonly associated with microalgae and zooplankton and produce the antibacterial compound tropodithietic acid. It is known to enhance host survival (i.e., fish eggs and larvae) and the viability of feed (rotifers, *Artemia*) (Dittmann et al. 2020; Sonnenschein et al. 2021). In the hindgut and hepatopancreas of juvenile palinurids, bacterial communities often include *Ruegeria* spp., which may enhance host resilience by deterring opportunistic pathogens, cycling sulfur and carbon, and forming protective biofilms (Ooi et al. 2023; Pereyra et al. 2025). Moreover, in probiotic screening experiments, *Ruegeria* spp. were among the isolates antagonistic toward the pathogenic

*V. owensii*, highlighting their potential as beneficial candidates in lobster larviculture (Goulden et al. 2012b). Additionally, *Portibacter* spp., a genus within the Bacteroidetes found in saline habitats and early jellyfish stages, was prevalent during the first few days and may be contributing to early bacterial stability (Peng et al. 2023; Yoon et al. 2012). Importantly, the bacterial composition observed at 0 dph could be interpreted as a "typical or baseline," resulting from the balance between the maternally retained microbiota and the contemporarily colonizing environmental bacteria sourced from the rearing system.

With the onset of WLD and mortality of *P. ornatus* larvae, we observed a significant shift in the bacterial community structure. Members of the Vibrionaceae, including the genus *Vibrio,* were constant in the larval bacterial communities throughout the sampling period. However, they became dominant at the early onset of the disease (8 dph), followed by a further transition to Flavobacteriaceae, particularly *Aquimarina* at 16 dph. These families are strongly associated with disease outbreaks in aquaculture, inducing septicaemia and tissue necrosis in crustaceans and fish (de Souza Valente and Wan 2021; Vandeputte et al. 2024). Some members of the genus *Vibrio* are well documented as opportunistic or primary pathogens in aquaculture, associated with vibriosis in species such as tiger prawn (*Penaeus monodon*) and crabs (*Brachyura* spp.) (Arunkumar et al. 2020; de Souza Valente and Wan 2021; Kim and Lee 2014). Furthermore, several species of *Vibrio* have been linked to lobster diseases; *V. owensii* in *P. ornatus*, *V. harveyi*, which causes hepatopancreatic necrosis in Caribbean spiny lobster (*Panulirus argus*) and eastern rock lobster (*Sagmariasus verreauxi)*, and *V. alginolyticus* and *V. damsela*, which act as opportunistic pathogens and are associated with disease under stress conditions (Diggles et al. 2000; Goulden et al. 2012a; Raissy et al. 2011; Rose et al. 2024). Some members of the Flavobacteriaceae are also associated with a range of economically damaging diseases in aquaculture, such as white faeces syndrome (WFS) in shrimp, columnaris in channel catfish (*Ictalurus punctatus*) and rainbow trout (*Oncorhynchus mykiss*), and ulcerative disease in Atlantic salmon (*Salmo salar*) (Avendaño-Herrera et al. 2006; Declercq et al. 2013; Kurniawinata et al. 2022). The genus *Aquimarina* was consistently detected throughout lobster development but was dominant during the disease peak. Strains within *Aquimarina* species have been shown to be causative agents of WLD in *P. ornatus* and scyllarid larvae, and cuticular diseases in American lobster (*Homarus americanus*) (Chistoserdov et al. 2012; Ooi et al. 2020). This temporal succession from beneficial to pathogenic taxa may reflect a destabilising process in the bacterial community. Significant changes in beta diversity across time points indicate increasing community instability, which may serve as a precursor to WLD onset in *P. ornatus* larvae.

Drivers of bacterial community shifts and the pathogenesis of WLD in *P. ornatus* larvae appear to arise from a complex interplay of several factors. At 0 dph, the larval bacterial community closely resembled those of the water and broodstock pleopods, suggesting possible maternal transmission in the latter case. However, this signal is likely confounded by immediate post-hatch environmental exposure, and the 0 dph communities may therefore represent a transitional microbiome influenced by both environmental and maternal sources. This pattern is also observed in the swimming crab (*Portunus trituberculatus*), where Rhodobacteraceae and Flavobacteriaceae are transmitted from broodstock to zoea (Sun et al. 2025). Furthermore, frequent moulting in crustaceans triggers metabolic and immune shifts that may destabilize the bacterial community, allowing opportunistic colonizers to dominate (Liu et al. 2022; Yuan et al. 2022; Zhang et al. 2021). In this study, the effects of moulting on bacterial community dynamics were likely overshadowed by the severe WLD outbreak, which may also have impaired the typical progression of moulting. Disruption during these periods can compromise bacterial

homeostasis and increase susceptibility to infection (Lin et al. 2024; Liu et al. 2022). However, from 1 to 16 dph, larval communities shifted, sharing bacteria with the rearing water, tank biofilm, and, especially, feed, highlighting a shift in detected bacterial sources from the early broodstock-associated to environmentally driven communities, reflecting colonization dynamics and environmental function in the rearing system. This mode of acquisition may increase the risk of dysbiosis, as environmental reservoirs can harbour opportunistic or fast-growing taxa (Egan and Gardiner 2016; Meres et al. 2012). Between 8 and 16 dph, coinciding with clinically apparent WLD, larval bacteria exhibited reduced diversity and succession towards *Vibrio* and *Aquimarina* dominance. Interestingly, we found a strong negative association between Vibrionaceae and Flavobacteriaceae, which suggests a structured ecological association between these taxa (Kern et al. 2021). *Vibrio* spp., as r-strategists, may exploit nutrient surges during moulting by producing enzymes that degrade chitin and mucus, and may be associated with dysbiosis by increasing population density and coordinating gene expression via quorum sensing (a cell-density-dependent signalling mechanism) (de Souza Valente and Wan 2021; Sharma and Gandhi 2024). The dysbiosis state may weaken host defences and further alter microbial stability (de Souza Valente and Wan 2021). Moreover, *Vibrio* can be positively associated with other fast-growing taxa, such as Marinobacteraceae and Oceanospirillaceae, potentially reflecting shared environmental responses rather than direct interactions (Hammerl et al. 2022; Nikolova and Gutierrez 2023; Speck and Donachie 2012; Zhang et al. 2023). In a dysregulated ecosystem, *Aquimarina* may exploit ecological niches through antagonistic traits, including enzyme production, adhesion, biofilm formation, and antimicrobial synthesis, which likely contribute to its persistence and relative dominance (Silva et al. 2022; Zhang et al. 2019; Zhu et al. 2022). Notably, *Aquimarina* was detected in broodstock, 0 dph larvae, rearing water, and consistently in feed samples across all time points (1–16 dph), indicating both maternal transmission and continuous acquisition from environmental sources. Its sustained presence in feed and rearing water suggests these may act as reservoirs, potentially contributing to the community shifts observed during WLD progression. However, its presence at low abundance in 0 dph larvae and consistent detection in feed and water suggests it may also function as an environmental opportunist that blooms under conditions of host stress and community destabilization. This pattern mirrors disease dynamics in other species. For example, in *L. vannamei*, *Vibrio* spp. levels in rearing water parallel those in infected shrimp during white faeces syndrome outbreaks (Kurniawinata et al. 2022), whereas in turbot (*Scophthalmus maximus*), environmental sources shape the gut communities and larval survival (Gómez and Balcázar 2008). Furthermore, bacteria may also positively or negatively correlate due to indirect reasons, based on their environmental preferences (Weiss et al. 2016). In microbial communities, positive or negative correlations may arise from shared environmental preferences, habitat differentiation, or host-associated niche partitioning (Faust and Raes 2012; Lima-Mendez et al. 2015; Steele et al. 2011). Therefore, it is possible that the observed negative association between Vibrionaceae and Flavobacteriaceae reflects ecological niche differentiation or other responses to environmental and host conditions during disease progression, rather than just direct competitive exclusion.

Finally, ultrastructural changes observed during the clinical signs of WLD were predominantly coagulative necrosis. This type of lesion is not specific to WLD and can be associated with infectious myonecrosis virus, *Penaeus vannamei* nodavirus (PvNV), and *Vibrio* spp. infections, often combined with environmental stressors. PvNV is an exotic disease in Australia that affects *L. vannamei*. Unlike our findings, it is usually accompanied

by haemolytic infiltration, viral inclusions in affected cells, and fibrosis (Huang et al. 2016). Bacterial muscle necrosis caused by *Vibrio* also results in infiltration of haemocytes into the muscle tissue, along with melanosis, muscle necrosis, and the presence of Gram-negative rods in the tissues (Intriago et al., 2024). The previous histopathological examination of white-leg diseased larvae showed proliferation of *Aquimarina* spp. beneath the chitinous cuticle of the pereiopods (Ooi et al. 2020), whereas this study did not observe bacterial cells or hemocytes. The reason may be that the earlier study involved an in vitro experimental challenge of older phyllosoma (16 dph) with a pure culture of *Aquimarina* spp. Alternatively, the necrotic changes could have resulted from *Aquimarina* colonizing the pereiopod's periphery and subsequent toxin production, thereby inducing myocyte damage in the absence of direct bacterial contact. An experimental challenge with a longitudinal sample collection would further elucidate WLD pathogenesis.

These findings reinforce that bacterial colonization in *P. ornatus* is not solely maternal/vertically acquired but is continuously shaped by environmental bacteria. Persistent exposure to unstable or pathogenic communities may predispose larvae to dysbiosis and the emergence of diseases such as WLD. White leg disease may reflect a stepwise process in which bacterial imbalance is associated with shifts in community structure, followed by increased representation of opportunistic taxa. This progression exemplifies a complex pathogenic model in which early microbiome disruption facilitates the sequential or synergistic actions of multiple bacterial taxa rather than a single pathogen and ultimately results in pathogen dominance and disease expression (Johnke et al. 2020; Kern et al. 2021; Stubbendieck et al. 2016).

This study was conducted under commercial-scale production conditions rather than controlled laboratory settings, which may introduce environmental variability and limit direct comparisons. Furthermore, the high mortality associated with the outbreak precluded the inclusion of contemporaneous healthy controls. Consequently, although significant shifts in alpha and beta diversity were observed during disease progression, these changes cannot be attributed exclusively to WLD and may also reflect broader host stress responses, declining physiological condition, or mortality-associated microbial succession. Therefore, the observed microbial community changes should be interpreted as being associated with disease progression during the outbreak rather than as definitive disease-specific signatures. Establishing a defined healthy baseline and incorporating appropriate control groups under control conditions would improve interpretation of bacterial dynamics and strengthen causal inference in future work. In addition, future studies incorporating measurements of feed-biofilm formation would provide a more comprehensive understanding of feed-associated microbial dynamics and disease progression. Finally, the DNA extraction method using a high-salt lysis buffer may be less efficient for Gram-positive taxa with thick cell walls; therefore, future studies could consider more robust extraction approaches, such as mechanical disruption or optimized commercial kits, to improve microbial representation.

## Conclusion

This study reveals that larval bacterial communities undergo significant shifts during the WLD outbreak in the commercial-scale lobster rearing system, with declining alpha diversity and fluctuating beta diversity indicating progressive bacterial destabilization. During the moulting process, larvae become physiologically vulnerable and more

susceptible to opportunistic infections. Early dominance by genera such as *Vibrio*, *Portibacter*, *Shimia*, and *Alteromonas* is replaced by a sudden increase in *Vibrio* and *Aquimarina* at 8 and 16 dph, respectively, preceding WLD onset. The observed bacterial succession from Vibrionaceae to Flavobacteriaceae, particularly *Aquimarina*, suggests potential bacterial interactions and shifts in community structure. These findings highlight the importance of maintaining bacterial balance to support a healthy aquaculture system and demonstrate that early bacterial disruption can facilitate disease emergence.

**Supplementary Information** The online version contains supplementary material available at https://doi.org/10.1007/s10499-026-02622-y.

**Acknowledgements** We would like to express my sincere appreciation to Mike William for his assistance with laboratory work, data analysis. We also wish to thank the IMAS aquaculture staff Adele Moyes, Kate Neil, Larnie Linton, Mathew Allen, Patricio Lillo Ramirez, Rhys Manchester, and Ross Goldsmid for culturing the lobsters and for their help in developing and maintaining the experimental systems.

**Author contributions** Mengjia Jiang: Writing—original draft; Andrew J. Trotter: Writing – review & editing, Supervision; Ivona Mladineo: Writing – review & editing, Supervision; Evan F. Goulden: Writing – review & editing, Supervision; Gregory G. Smith: review & editing, project administration. All authors have read and agreed to the published version of the manuscript.

**Funding** This work was undertaken by the Australian Research Council Industrial Transformation Hub for Sustainable Onshore Lobster Aquaculture (project number IH190100014). Views expressed herein are those of the authors and not necessarily those of the Australian Government or Australian Research Council.

**Data availability** The datasets generated and/or analysed during the current study are available from the corresponding author on request.

## Declarations

**Competing interests** The authors declare no competing interests.



## References

Anderson MJ (2001) A new method for non-parametric multivariate analysis of variance. Austral Ecol 26:32–46

Anderson MJ (2006) Distance-based tests for homogeneity of multivariate dispersions. Biometrics 62:245–253

Angthong P, Chaiyapechara S, Rungrassamee W (2023) Shrimp microbiome and immune development in the early life stages. Dev Comp Immunol 147:104765

Arbizu M (2020) pairwiseAdonis: pairwise multilevel comparison using adonis. R package. *In* Version 0.4. Available on URL: https://github.com/pmartinezarbizu/pairwiseAdonis. Accessed 5 Jan 2026

Arunkumar M, LewisOscar F, Thajuddin N, Pugazhendhi A, Nithya C (2020) In *vitro* and in *vivo* biofilm forming *Vibrio* spp: a significant threat in aquaculture. Process Biochem 94:213–223

Avendaño-Herrera R, Toranzo AE, Magariños B (2006) Tenacibaculosis infection in marine fish caused by *Tenacibaculum maritimum*: a review. Dis Aquat Org 71:255–266
Benjamini Y, Hochberg Y (1995) Controlling the false discovery rate: a practical and powerful approach to multiple testing. J R Stat Soc Ser B Stat Methodol 57:289–300
Bourne D, Høj L, Webster N, Payne M, Skindersøe M, Givskov M, Hall M (2007) Microbiological aspects of phyllosoma rearing of the ornate rock lobster *Panulirus ornatus*. Aquaculture 268:274–287
Cassol I, Ibañez M, Bustamante JP (2025) Key features and guidelines for the application of microbial alpha diversity metrics. Sci Rep 15:622
Chistoserdov AY, Quinn RA, Gubbala SL, Smolowitz R (2012) Bacterial communities associated with lesions of shell disease in the American lobster, *Homarus americanus* Milne-Edwards. J Shellfish Res 31:449–462
Curry KD, Wang Q, Nute MG, Tyshaieva A, Reeves E, Soriano S, Wu Q, Graeber E, Finzer P, Mendling W (2022) Emu: species-level microbial community profiling of full-length 16S rRNA Oxford Nanopore sequencing data. Nat Methods 19:845–853
Curry KD, Soriano S, Nute MG, Villapol S, Dilthey A, Treangen TJ (2024) Microbial community profiling protocol with full-length 16S rRNA Sequences and EMU. Current Protocols 4:e978
Dai W, Sheng Z, Chen J, Xiong J (2020) Shrimp disease progression increases the gut bacterial network complexity and abundances of keystone taxa. Aquaculture 517:734802
de Souza Valente C, Wan AH (2021) *Vibrio* and major commercially important vibriosis diseases in decapod crustaceans. J Invertebr Pathol 181:107527
Declercq AM, Haesebrouck F, Van den Broeck W, Bossier P, Decostere A (2013) Columnaris disease in fish: a review with emphasis on bacterium-host interactions. Vet Res 44:1–17
Diggles B, Moss G, Carson J, Anderson C (2000) Luminous vibriosis in rock lobster *Jasus verreauxi* (Decapoda: Palinuridae) phyllosoma larvae associated with infection by *Vibrio harveyi*. Dis Aquat Organ 43:127–137
Dittmann KK, Rasmussen BB, Melchiorsen J, Sonnenschein EC, Gram L, Bentzon-Tilia M (2020) Changes in the microbiome of mariculture feed organisms after treatment with a potentially probiotic strain of *Phaeobacter inhibens*. Appl Environ Microbiol 86:e00499–00420
Driscoll J, Boyd C, Tyedmers P (2015) Life cycle assessment of the Maine and southwest Nova Scotia lobster industries. Fish Res 172:385–400
Egan S, Gardiner M (2016) Microbial dysbiosis: rethinking disease in marine ecosystems. Front Microbiol 7:991
FAO (2024) The State of Food and Agriculture 2024: Value-driven transformation of agrifood systems. Food and Agriculture Organization of the United Nations, Rome, Italy. https://doi.org/10.4060/cd2616en
Faust K, Raes J (2012) Microbial interactions: from networks to models. Nat Rev Microbiol 10:538–550
Feinman SG, Martínez AU, Bowen JL, Tlusty MF (2017) Fine-scale transition to lower bacterial diversity and altered community composition precedes shell disease in laboratory-reared juvenile American lobster. Dis Aquat Organ 124:41–54
Francis DS, Salmon ML, Kenway MJ, Hall MR (2014) Palinurid lobster aquaculture: nutritional progress and considerations for successful larval rearing. Rev Aquac 6:180–203
Gómez GD, Balcázar JL (2008) A review on the interactions between gut microbiota and innate immunity of fish. FEMS Immunol Med Microbiol 52:145–154
Goulden EF, Hall MR, Bourne DG, Pereg LL, Høj L (2012) Pathogenicity and infection cycle of *Vibrio owensii* in larviculture of the ornate spiny lobster (*Panulirus ornatus)*. Appl Environ Microbiol 78:2841–2849
Goulden EF, Hall MR, Pereg LL, Høj L (2012) Identification of an antagonistic probiotic combination protecting ornate spiny lobster (*Panulirus ornatus*) larvae against *Vibrio owensii* infection. PLoS One 7:e39667
Goulden EF, Høj L, Hall MR (2013) Microbial management for bacterial pathogen control in invertebrate aquaculture hatcheries. In: Allan G, Burnell G (eds) Advances in Aquaculture Hatchery Technology. Woodhead Publishing, Oxford, UK, pp 246–285. https://doi.org/10.1533/9780857097460.1.246
Hammerl JA, Ritchie JM, Leoni F, Banerjee S, Strauch E (2022) Molecular adaptations of vibrionaceae to changing environments, volume II. Front Microbiol 13:863038
Hasegawa H, Naganuma K, Nakagawa Y, Matsuyama T (2003) Membrane filter (pore size, 0.22–0.45 μm; thickness, 150 μm) passing-through activity of *Pseudomonas aeruginosa* and other bacterial species with indigenous infiltration ability. Federat Eur Microbiol Soc Microbiol Lett 223:41–46
Heberle H, Meirelles GV, da Silva FR, Telles GP, Minghim R (2015) InteractiVenn: a web-based tool for the analysis of sets through Venn diagrams. BioMed Central Bioinform 16:1–7

Huang Z, Li X, Wang L, Shao Z (2016) Changes in the intestinal bacterial community during the growth of white shrimp, *Litopenaeus vannamei*. Aquac Res 47:1737–1746

Hyun D-W, Kim M-S, Shin N-R, Kim JY, Kim PS, Whon TW, Yun J-H, Bae J-W (2013) *Shimia haliotis* sp. nov., a bacterium isolated from the gut of an abalone, *Haliotis discus hannai*. Int J Syst Evol Microbiol 63:4248–4253

Intriago P, Montiel B, Valarezo M, Arteaga K, Romero X, Montenegro A (2024) Bacterial muscle necrosis in cultured Penaeus vannamei in latin America. Aquacult Res. 2024:9919229.

Johnke J, Fraune S, Bosch TC, Hentschel U, Schulenburg H (2020) *Bdellovibrio* and like organisms are predictors of microbiome diversity in distinct host groups. Microb Ecol 79:252–257

Kassambara A (2019) rstatix: pipe-friendly framework for basic statistical tests. R package, version 0.7.0. https://doi.org/10.32614/CRAN.package.rstatix

Kern L, Abdeen SK, Kolodziejczyk AA, Elinav E (2021) Commensal inter-bacterial interactions shaping the microbiota. Curr Opin Microbiol 63:158–171

Kim JY, Lee JL (2014) Multipurpose assessment for the quantification of *Vibrio* spp. and total bacteria in fish and seawater using multiplex real-time polymerase chain reaction. J Sci Food Agric 94:2807–2817

Kurniawinata MI, Sukenda S, Wahjuningrum D, Widanarni W (2022) Bacterial diversity and community composition in the gut and rearing water of Pacific white shrimp *Penaeus vannamei* during an outbreak of white feces disease. Aquaculture 559:738431

Lewis CL, Glendinning S, Codabaccus BM, Carter CG, Fitzgibbon QP, Smith GG, Elizur A, Ventura T (2024) Changes in the physiology and chitin metabolism in cultured juvenile *Panulirus ornatus* across the moult cycle. Aquac Rep 38:102308

Li T, Long M, Ji C, Shen Z, Gatesoupe F-J, Zhang X, Zhang Q, Zhang L, Zhao Y, Liu X (2016) Alterations of the gut microbiome of largemouth bronze gudgeon (*Coreius guichenoti*) suffering from furunculosis. Sci Rep 6:30606

Lima-Mendez G, Faust K, Henry N, Decelle J, Colin S, Carcillo F, Chaffron S, Ignacio-Espinosa JC, Roux S, Vincent F (2015) Determinants of community structure in the global plankton interactome. Science 348:1262073

Lin W, Chen J, Shi C, Mu C, Wang C, Ye Y (2024) Reassembly and biotic sources of carapace bacterial community of *Portunus trituberculatus* after host molting. Aquaculture 587:740863

Liu M, Ni H, Zhang X, Sun Q, Wu X, He J (2022) Comparative transcriptomics reveals the immune dynamics during the molting cycle of swimming crab *Portunus trituberculatus*. Front Immunol 13:1037739

Lu Z, Ren Z, Lin W, Shi C, Mu C, Wang C, Wu Q, Ye Y (2022) Succession, sources, and assembly of bacterial community in the developing crab larval microbiome. Aquaculture 548:737600

Lu Y, Zhou G, Ewald J, Pang Z, Shiri T, Xia J (2023) MicrobiomeAnalyst 2.0: comprehensive statistical, functional and integrative analysis of microbiome data. Nucleic Acids Res 51:W310–W318

Matsuo Y (2023) Full-length 16S rRNA gene analysis using long-read nanopore sequencing for rapid identification of bacteria from clinical specimens. In: Arakawa K (ed) Nanopore sequencing: methods and protocols. Methods in Molecular Biology, vol 2632. Humana, New York, Springer, pp 193–213. https://doi.org/10.1007/978-1-0716-2996-3_14

Meres NJ, Ajuzie CC, Sikaroodi M, Vemulapalli M, Shields JD, Gillevet PM (2012) Dysbiosis in epizootic shell disease of the American lobster (*Homarus americanus*). J Shellfish Res 31:463–472

Midorikawa Y, Shimizu T, Sanda T, Hamasaki K, Dan S, Lal MTBM, Kato G, Sano M (2020) Characterization of *Aquimarina hainanensis* isolated from diseased mud crab *Scylla serrata* larvae in a hatchery. J Fish Dis 43:541–549

Nikolova C, Gutierrez T (2023) Novel approaches in the use of biosurfactants in the oil industry and environmental remediation. Biosurfactants. In: Soberón-Chávez G (ed) Biosurfactants: Research and Development. Elsevier, pp 107–128. https://doi.org/10.1016/B978-0-323-91697-4.00006-5

Oksanen J, Simpson GL, Blanchet FG, Kindt R, Legendre P, Minchin PR, O'Hara RB, Solymos P, Stevens MHH, Szoecs E, Wagner H, Barbour M, Bedward M, Bolker B, Borcard D, Borman T, Carvalho G, Chirico M, Caceres MD, Durand S, Evangelista HBA, FitzJohn R, Friendly M, Furneaux B, Hannigan G, Hill MO, Lahti L, Martino C, McGlinn D, Ouellette M-H, Cunha ER, Smith T, Stier A, Braak CJFT, Weedon J (2025) Vegan: community ecology package. R package, version 2.7.1. https://doi.org/10.32614/CRAN.package.vegan. Accessed 12 Dec 2025

Ooi MC, Goulden EF, Trotter AJ, Smith GG, Bridle AR (2020) *Aquimarina* sp. associated with a cuticular disease of cultured larval palinurid and scyllarid lobsters. Front Microbiol 11:573588

Ooi MC, Trotter AJ, Smith GG, Bridle AR (2023) Characterisation of the gut bacteria of cultured and wild spiny lobster. Appl Microbiol 3:241–253

Payne MS, Hall MR, Sly L, Bourne DG (2007) Microbial diversity within early-stage cultured *Panulirus ornatus* phyllosomas. Appl Environ Microbiol 73:1940–1951

Payne M, Høj L, Wietz M, Hall M, Sly L, Bourne D (2008) Microbial diversity of mid-stage *Palinurid phyllosoma* from Great Barrier Reef waters. J Appl Microbiol 105:340–350
Peng S, Ye L, Li Y, Wang F, Sun T, Wang L, Hao W, Zhao J, Dong Z (2023) Microbiota regulates life-cycle transition and nematocyte dynamics in jellyfish. iScience. https://doi.org/10.1016/j.isci.2023.108444
Pereyra JPA, Loh AAR, Hu D, Deignan LK, Summers S, Case RJ (2025) Draft genomes of two *Ruegeria* spp. isolated from the coral species *Pachyseris speciosa* in Singapore. Microbiol Resour Announce 14:e01303-01324
Raissy M, Momtaz H, Moumeni M, Ansari M, Rahimi E (2011) Molecular detection of Vibrio spp. in lobster hemolymph. Afr J Microbiol Res 5:1697–1700
Rajeev M, Jung I, Kang I, Cho J-C (2024) Genome-centric metagenomics provides insights into the core microbial community and functional profiles of biofloc aquaculture. Msystems 9:e00782-00724
Rose D, Bennett H, Dill-Okubo J, Francis-Floyd R, Camus AC, Waldbieser GC, Griffin MJ (2024) Complete genome of *Vibrio harveyi* isolate K2014767 from the hepatopancreas of captive Caribbean spiny lobster (*Panulirus argus*). Microbiol Resour Announce 13:e01156-01123
Sharma S, Gandhi SG (2024) Quorum sensing and its role in bacterial pathogenicity. In: Verma PK, Mishra S, Srivastava V, Mehrotra S (eds) Plant Pathogen Interaction. Springer, Singapore. https://doi.org/10.1007/978-981-99-4890-1_8
Shi Y, Zhang L, Do K-A, Peterson CB, Jenq RR (2020) aPCoA: covariate adjusted principal coordinates analysis. Bioinformatics 36:4099–4101
Silva SG, Paula P, Da Silva JP, Mil-Homens D, Teixeira MC, Fialho AM, Costa R, Keller-Costa T (2022) Insights into the antimicrobial activities and metabolomes of *Aquimarina* (Flavobacteriaceae, Bacteroidetes) species from the rare marine biosphere. Mar Drugs 20:423
Sonnenschein EC, Jimenez G, Castex M, Gram L (2021) The *Roseobacter*-group bacterium *Phaeobacter* as a safe probiotic solution for aquaculture. Appl Environ Microbiol 87:e02581–e02520
Speck MD, Donachie SP (2012) Widespread Oceanospirillaceae bacteria in *porites* spp. J Mar Sci 2012:746720
Steele JA, Countway PD, Xia L, Vigil PD, Beman JM, Kim DY, Chow C-ET, Sachdeva R, Jones AC, Schwalbach MS (2011) Marine bacterial, archaeal and protistan association networks reveal ecological linkages. ISME J 5:1414–1425
Stubbendieck RM, Vargas-Bautista C, Straight PD (2016) Bacterial communities: interactions to scale. Front Microbiol 7:1234
Sun Y, Lin W, Wu Q, Shi C, Wang C, Ye Y (2025) Bacterial dynamics and biotic sources in the developing swimming crab embryos. Aquaculture 595:741523
Vandeputte M, Kashem MA, Bossier P, Vanrompay D (2024) *Vibrio* pathogens and their toxins in aquaculture: a comprehensive review. Rev Aquac 16:1858–1878
Wang Y, Hammes F, Boon N, Egli T (2007) Quantification of the filterability of freshwater bacteria through 0.45, 0.22, and 0.1 µm pore size filters and shape-dependent enrichment of filterable bacterial communities. Environ Sci Technol 41:7080–7086
Weiss S, Van Treuren W, Lozupone C, Faust K, Friedman J, Deng Y, Xia LC, Xu ZZ, Ursell L, Alm EJ (2016) Correlation detection strategies in microbial data sets vary widely in sensitivity and precision. ISME J 10:1669–1681
Wickham H, Chang W, Henry L, Pedersen TL, Takahashi K, Wilke C, Woo K, Yutani H, Dunnington D, van den Brand T (2025) Data analysis. In: Wickham H, Navarro D, Pedersen TL (eds) ggplot2: Elegant Graphics for Data Analysis. Springer, Cham. https://ggplot2-book.org/
Xiong J, Zhu J, Dai W, Dong C, Qiu Q, Li C (2017) Integrating gut microbiota immaturity and disease-discriminatory taxa to diagnose the initiation and severity of shrimp disease. Environ Microbiol 19:1490–1501
Xiong J-B, Nie L, Chen J (2018) Current understanding on the roles of gut microbiota in fish disease and immunity. Zool Res 40:70
Xiong J, Dai W, Qiu Q, Zhu J, Yang W, Li C (2018) Response of host–bacterial colonization in shrimp to developmental stage, environment and disease. Mol Ecol 27:3686–3699
Yoon J, Matsuo Y, Kasai H, Yokota A (2012) *Portibacter lacus* gen. nov., sp. nov., a new member of the family *Saprospiraceae* isolated from a saline lake. J Gen Appl Microbiol 58:191–197
Yuan Y, Jin M, Fang F, Tocher DR, Betancor MB, Jiao L, Hong Y, Zhou Q (2022) New insight into the molting and growth in crustaceans: regulation of energy homeostasis through the lipid nutrition. Front Mar Sci 9:914590
Zhang S, Sun X (2022) Core gut microbiota of shrimp function as a regulator to maintain immune homeostasis in response to WSSV infection. Microbiol Spectr 10:e02465–02421

Zhang Z, Lv Z, Zhang W, Shao Y, Zhao X, Guo M, Li C (2019) Comparative analysis of midgut bacterial community under *Vibrio splendidus* infection in *Apostichopus japonicus* with hindgut as a reference. Aquaculture 513:734427

Zhang C, Xiu L, Li Y, Sun L, Li Y, Zeng Y, Wang F, Peng J (2021) Multiplex PCR and nanopore sequencing of genes associated with antimicrobial resistance in *Neisseria gonorrhoeae* directly from clinical samples. Clin Chem 67:610–620

Zhang W, Liu Y, Zheng K, Xing J, Li Q, Gu C, Wang Z, Shao H, Guo C, He H (2023) Discovery of an abundant viral genus in polar regions through the isolation and genomic characterization of a new virus against *Oceanospirillaceae*. Appl Environ Microbiol 89:e01896–01822

Zhu X, Ji L, Cheng M, Wei H, Wang Z, Ning K (2022) Sustainability of the rice-crayfish co-culture aquaculture model: microbiome profiles based on multi-kingdom analyses. Environ Microbiol 17:27